Int J Thermophys (2016) 37:97
DOI 10.1007/s10765-016-2102-9

ICPPP 18

Detection of Fiber Layer-Up Lamination Order of CFRP Composite Using Thermal-Wave Radar Imaging

Fei Wang[1,2,3] · Junyan Liu[1,2,3] · Yang Liu[1,2,3] · Yang Wang[1,2,3] · Jinlong Gong[1,2,3]

Received: 20 September 2015 / Accepted: 11 July 2016 / Published online: 27 July 2016

Abstract In this paper, thermal-wave radar imaging (TWRI) is used as a non-destructive inspection method to evaluate carbon-fiber-reinforced-polymer (CFRP) composite. An inverse methodology that combines TWRI with numerical optimization technique is proposed to determine the fiber layer-up lamination sequences of anisotropic CFRP composite. A 7-layer CFRP laminate $[0°/45°/90°/0°]_s$ is heated by a chirp-modulated Gaussian laser beam, and then finite element method (FEM) is employed to calculate the temperature field of CFRP laminates. The phase based on lock-in correlation between reference chirp signal and the thermal-wave signal is performed to obtain the phase image of TWRI, and the least square method is applied to reconstruct the cost function that minimizes the square of the difference between the phase of TWRI inspection and numerical calculation. A hybrid algorithm that combines the simulation annealing with Nelder–Mead simplex research method is employed to solve the reconstructed cost function and find the global optimal solution of the layer-up sequences of CFRP composite. The result shows the feasibility of estimating the fiber layer-up lamination sequences of CFRP composite with optimal discrete and constraint conditions.

This article is part of the selected papers presented at the 18th International Conference on Photoacoustic and Photothermal Phenomena.

✉ Yang Wang
wyyh@hit.edu.cn

1 State Key Laboratory of Robotics and System (HIT), Harbin 150001, People's Republic of China

2 School of Mechatronics Engineering, Harbin Institute of Technology, Harbin 150001, People's Republic of China

3 Xidazhi Street 92#, Nangang District, Harbin 150001, Heilongjiang province, People's Republic of China

Keywords CFRP · Finite element method · Infrared thermography · Lay-up sequence

1 Introduction

Carbon-fiber-reinforced polymer (CFRP), a kind of novel composite material, has the merits of high-specific strength, high-specific modulus and anti-fatigue performances, which lead to the wide application of CFRP in the fields of aircraft, aerospace, petrochemical, automotive and military industries. CFRP laminate is a classical material whose nondestructive material property characterization is as important as flaw detection [1]. Fiber-reinforced composite laminates often possess strong in-plane elastic anisotropy due to its specific fiber lay-up orientations and sequences. However, one of the most important factors is the ply sequence or orientation which can directly affect the structure performance of CFRP composite. If one ply is misaligned in the lay-up sequences, it can be drastically alternative to the mechanical performance of CFRP laminates. Therefore, in most cases, a small sample is cut from the waste edge, and then its orientation or sequence is verified by an optical microscope in a Lab [2]. As the order of the lay-up is very essential for the CFRP panels, the depth-resolved determination of fiber lay-up sequences is a significantly challenging task for nondestructive testing and evaluation (NDT&E) [3]. Active infrared thermography is a new nondestructive testing method with an increasing range of applications [4–11]. A theoretical model for the measurement of fiber orientations with thermal wave has been proposed and deeply studied by Karpen et al. [3], and the anisotropy induced by fibers resulted in elliptical contour lines of phase angle or amplitude image of lock-in thermography (LIT). The direction and eccentricity of elliptical contour lines are correlated with the orientation of fibers and the corresponding degree of thermal anisotropy, respectively. Recently, combining linear frequency-modulated continuous wave radar with frequency-domain photothermal radiometry (PTR), a novel thermal-wave radar imaging (TWRI) has been developed to detect human dental demineralization lesions and osteoporotic bone loss [12,13]. TWRI methodology suggests a significant improvement in depth-resolution dynamic range of subsurface defects. In this work, an inverse analysis approach that combines TWRI with numerical simulation technique is proposed for the purpose of nondestructively determining the fiber layer-up lamination sequences of anisotropic CFRP composite.

2 Principle of Technique

2.1 Direct Problem

Figure 1 shows the diagram of TWRI for determining the lay-up sequences of CFRP laminates. The orthogonal global coordinate system xyz is rotated from the principal direction of a single ply. Assuming a rotation angle θ_n of both x and y axes (the $x - y$ plane coincides with the composite laminate plane), the general heat diffusion equation expression for a single ply composite becomes [14],

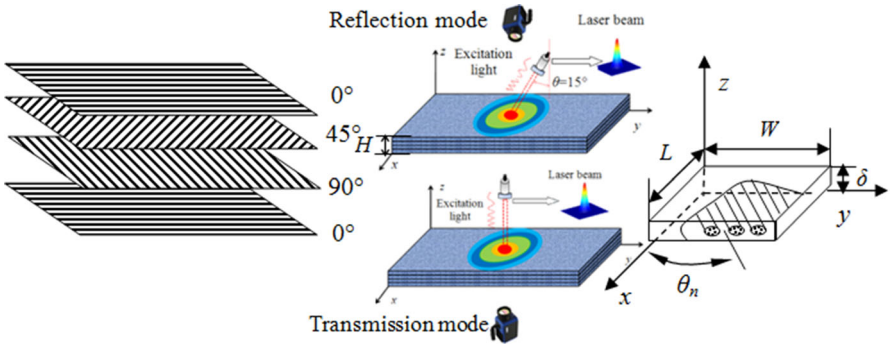

Fig. 1 The diagram of TWRI for the determination lay-up sequence of CFRP laminates

$$k_{nxx}\frac{\partial^2 T(x,y,z,t)}{\partial x^2}+k_{nyy}\frac{\partial^2 T(x,y,z,t)}{\partial y^2} +k_{nzz}\frac{\partial^2 T(x,y,z,t)}{\partial z^2}+2k_{nxy}\frac{\partial^2 T(x,y,z,t)}{\partial x\partial y}=\rho c_p\frac{\partial T(x,y,z,t)}{\partial t} \tag{1}$$

with,

$$k_{nxx}=k_{//}\cos^2(\theta_n)+k_{\perp}\sin^2(\theta_n) \tag{2}$$

$$k_{nyy}=k_{//}\sin^2(\theta_n)+k_{\perp}\cos^2(\theta_n) \tag{3}$$

$$k_{nxy}=k_{nyx}=(k_{//}-k_{\perp})\sin(\theta_n)\cos(\theta_n) \tag{4}$$

$$k_{nzz}=k_{\perp} \tag{5}$$

here, $k_{//}, k_{\perp}$ present the thermal conductivity value parallel and perpendicular to the fibers, $k_{nxx}, k_{nyy}, k_{nzz}$ denote the thermal conductivity tensors of x, y, z direction of the n layer in the global coordinate system, k_{nxy}, k_{nyx} are the thermal conductivity tensors of xy plane of the n layer in the global coordinate system, and θ_n is the laying-up angle of the n layer in the global coordinate system.

A laser of Gaussian distribution intensity is used as an external excitation source, and the laser beam spot size can change during the TWRI inspection. Assuming no consideration of optical absorption, the heat flux on the surface is given by,

$$q(x,y,t)=\frac{P}{\pi d^2}\exp\left[-\frac{(x-x_0)^2+(y-y_0)^2}{(d/2)^2}\right]\left\{1-\cos\left[\left(f_0+\frac{f_e-f_0}{T_s}t\right)t\right]\right\} \tag{6}$$

where $q(x, y, t)$ presents the excitation heat flux, x_0 and y_0 are the xy plane coordinates of the laser spot center, P, d are the laser power peak value and spot size, and f_0, f_e denote the chirp starting and ending frequency. T_s is the chirp scanning period.

The initial condition is defined by Eq. 7:

$$T(x,y,z,0)=T_{am} \tag{7}$$

The heat flux continuity condition is defined by Eq. 8:

$$-k_{nzz}\frac{dT(x,y,z,t)}{dz}|_{z=n\delta} = -k_{(n+1)zz}\frac{dT(x,y,z,t)}{dz}|_{z=n\delta}$$
$$0 \le x \le L, \quad 0 \le y \le W, \quad t > 0 \tag{8}$$

The boundary conditions, including the heat transfer by convection and radiation between the sample surfaces and the ambient environment, are defined by Eq. 9:

$$-k_{1zz}\frac{dT(x,y,z,t)}{dz}|_{z=0} = q(x,y,t) + h\left[T_{am} - T(x,y,0,t)\right] + \varepsilon\sigma\left[T_{am}^4 - T(x,y,0,t)^4\right]$$
$$0 \le x \le L, \quad 0 \le y \le W, \quad t > 0 \tag{9a}$$
$$-k_{Nzz}\frac{dT(x,y,z,t)}{dz}|_{z=H} = h\left[T_{am} - T(x,y,H,t)\right] + \varepsilon\sigma\left[T_{am}^4 - T(x,y,H,t)^4\right]$$
$$0 \le x \le L, \quad 0 \le y \le W, \quad t > 0 \tag{9b}$$

In Eqs. 7 and 9, T_∞ is the ambient temperature assuming that the air and the external environment are at the same temperature. N is the total number of layers, h, ε, σ are the natural convection heat transfer coefficient, the surface emissivity and Stefan–Boltzmann constant, respectively.

The temperature distribution of the irradiated surface (reflection mode) or the opposite surface (transmission mode) is captured by an IR camera, and the thermal-wave radar signal T_{TWR} derives from subtracting the temporal mean component from the surface temperature [15]. Like the digital lock-in correlation algorithm, the chirp signal is used as the reference signal instead of sinusoidal signal, so the following expressions are given by

$$S^0 = \frac{1}{N}\sum_{n=1}^{N-1}\left(T_{TWR}(n)\cos\left\{2\pi\left[\frac{f_0}{f_s}n + \left(\frac{f_e - f_0}{T_s}\right)\frac{n^2}{f_s^2}\right]\right\}\right) \tag{10}$$

$$S^{90} = \frac{1}{N}\sum_{n=1}^{N-1}\left(T_{TWR}(n)\sin\left\{2\pi\left[\frac{f_0}{f_s}n + \left(\frac{f_e - f_0}{T_s}\right)\frac{n^2}{f_s^2}\right]\right\}\right) \tag{11}$$

where f_s denotes the frame rate of the IR camera, and S^0 and S^{90} are, respectively, the co-called the in-phase and quadrature signal output. Then, the amplitude and phase are, respectively, computed by,

$$Am = \sqrt{\left(S^0\right)^2 + \left(S^{90}\right)^2} \tag{12}$$

$$Ph = \arctan\left(\frac{S^{90}}{S^0}\right) \tag{13}$$

The finite element method (FEM) is applied to solve the direct problem with consideration of the corresponding boundary and initial conditions, and the FEM is performed with ABAQUS 6.2.

2.2 The Inverse Analysis

Information on amplitude and phase images formed during TWRI could be used to extract the quantitative characteristics of the fiber lay-up orientations in the tested material. Generally, the phase characteristic of the thermal wave has the advantages of less sensitive to non-uniform heating and surface emissivity variation in comparison with the amplitude [16–18]. Therefore, in this case, the determination process can be performed through inversely solving the constructed objective function by the phase distribution, which uses the experimental phase distribution to estimate the fiber lay-up sequences in the test sample. An objective function is defined as a sum of squared differences between the measured phase distribution of the thermal wave and those from the computational results using guessed or estimated solutions as follows,

$$f(p) = \frac{1}{M^2} \sum_{i=1}^{M} \sum_{j=1}^{M} \left[Ph(x_i, y_j, 0, p) - Ph(x_i, y_j, 0)_{\mathrm{TWRI}} \right]^2 \tag{14}$$

and

$$p = [p_1 \quad p_2 \quad \ldots \quad p_n]^T = [\theta_1 \quad \theta_2 \quad \ldots \quad \theta_n]^T \tag{15}$$

where $f(p)$ is the objective function, $Ph(x_i, y_j, 0, p), i, j = 1, 2, \ldots M$, represents the phase distribution of TWRI from direct problem using estimated solutions, and $Ph(x_i, y_j, 0)_{\mathrm{TWRI}}, i, j = 1, 2, \ldots M$, denotes the measured phase distribution at the same locations using TWRI. Then the inverse problem can be recast as the following discrete location optimization problem, where the cost function is defined as Eq. 16, and the desired system parameters, $\theta_1, \theta_2, \ldots, \theta_n$, are determined by minimizing the cost function,

$$\min[f(p)] = \min \left\{ \frac{1}{M^2} \sum_{i=1}^{M} \sum_{j=1}^{M} \left[Ph(x_i, y_j, 0, p) - Ph(x_i, y_j, 0)_{\mathrm{TWRI}} \right]^2 \right\} \tag{16}$$

A hybrid optimization method which integrates simulation annealing algorithm (SA) into Nelder–Mead simplex search method (NM) [19] is employed to solve the Eq. 16. Two levels of stopping criteria are adopted in the hybrid method, the first one is to check whether a predefined objective function value or a predefined maximum number of iterations has reached for the SA, and then the search procedure should change to the NM to find the optimal solution. Finally, the second-level convergence criterion is employed to control the termination of the optimization procedure. The optimization process is terminated if one of the two conditions is satisfied: The desired value of the objective function is reached up; or the objective function value has no apparent improvement for a specified maximum number of iterations.

2.3 Experimental Procedures

2.3.1 Specimen and Properties

In this investigation, a CFRP (T300) laminate specimen was manufactured by symmetry cross-ply 7 layers by Spaceflight Materials and Technology Research Institute (SMTRI), and the fiber lay-up was the form of $[0°/45°/90°/0°]_s$. The single-layer thickness is about 0.3 mm, and the total thickness of multilayer CFRP laminates is about 2.1 mm. The thermal properties of single-layer CFRP material were given by the manufacturer (the thermal conductivities $k_{//} \approx 4.071\ \mathrm{W \cdot m^{-1} \cdot K^{-1}}$, $k_{\perp} \approx 0.776\ \mathrm{W \cdot m^{-1} \cdot K^{-1}}$ and the specific heat $c_p \approx 846.64\ \mathrm{J \cdot kg^{-1} \cdot K^{-1}}$ at room temperature 25 °C), and the density of CFRP sample was directly measured as $\rho = 1550\ \mathrm{kg \cdot m^{-3}}$. The size of the CFRP laminate specimen is constant at $40 \times 40\ \mathrm{mm^2}$.

2.3.2 Experimental Setup and Procedure

According to the methodology above, the TWRI system is developed as Fig. 2. A fiber-coupled 808 nm diode laser is applied as an excitation source, and a data acquisition module NI6229 from National Instruments is used to generate the chirp waveform for laser current. The IR camera is FLIR SC 7000, which is a Stirling cooled camera with 320×256 array of 3.6 μm–5.1 μm InSb detectors, and it is located in the opposite position from the laser excitation. The camera images are read by the computer using the DAQ card, and a homemade software developed by Labview programming is employed for the implementation of digital lock-in correlation computation. The chirp-modulated parameters are selected as $f_0 = 0.05$ Hz, $f_e = 0.01$ Hz and $T_s = 100$ s, the laser power peak value and the spot size are set to 300 mW and 10 mm, respectively, and the excitation duration is set to 400 s. The angle of the fiber lay-up orientation for each layer is set from 0° to 180°. The maximum iterations of SA is fixed at 50 iterations, and its initial annealing temperature is set to 500 °C. Then the search procedure changes to NM to find the optimal solution, and the maximum iteration of NM is set to 40 iterations.

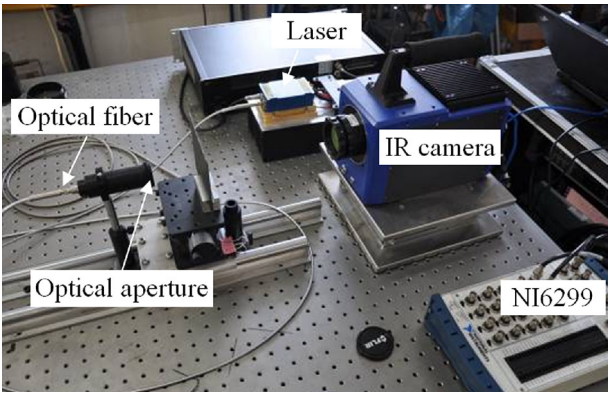

Fig. 2 TWRI setup

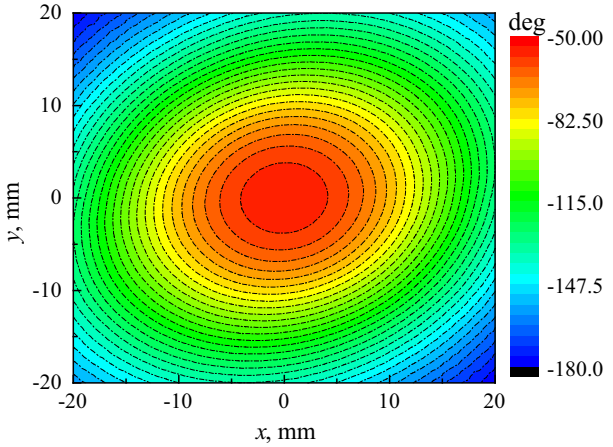

Fig. 3 TWRI phase distribution

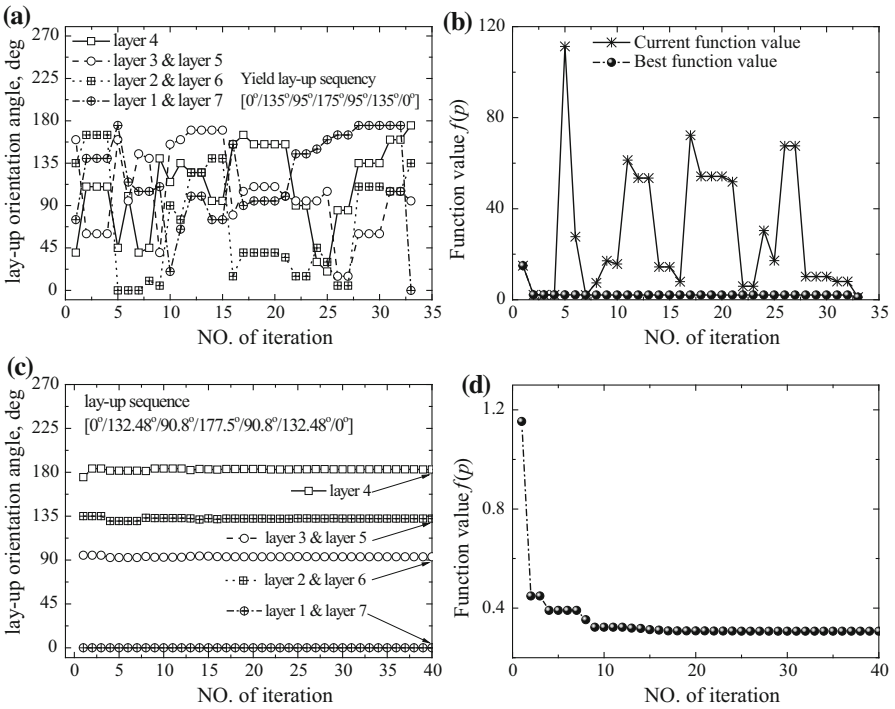

Fig. 4 Convergence tests for the fiber lay-up sequence: (a) searching process by SA, (b) the objection function value variations by SA, (c) searching process by NM, and (d) the objection function value variations by NM

Table 1 Experimental estimation of fiber lay-up orientation sequence of CFRP laminates through inverse solving the objective function Eq. 14 by the hybrid method (SA+NM)

Trails	Layer #1 and layer #7		Layer #2 and layer #6		Layer #3 and layer #5		Layer #4	
	Exact	Difference	Exact	Difference	Exact	Difference	Exact	Difference
	0°(180°)	–	45°(135°)	–	90°	–	0°(180°)	–
#1	0	0	132.57	2.43	91.95	1.95	0	0
#2	0	0	133.02	1.98	88.26	−1.74	178.19	−1.81
#3	0	0	132.48	2.52	90.81	0.81	177.5	−2.5
#4	0	0	132.40	2.60	94.06	4.06	4.50	4.50
#5	0	0	132.54	2.46	94.53	4.53	4.35	4.35

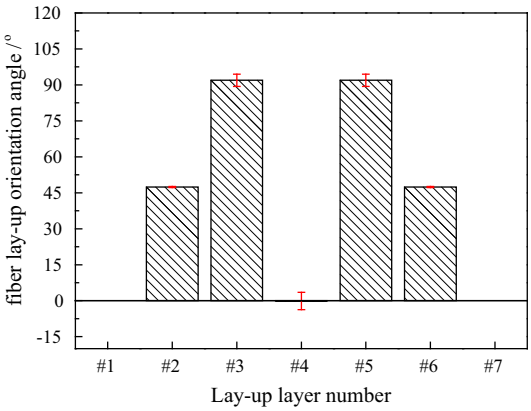

Fig. 5 The mean value and standard deviation of fiber lay-up orientation angle

3 Results

Figure 3 presents the TWRI lock-in phasegrams. It can be seen that the TWRI lock-in phase distribution contour lines can be approximated as ellipses, and the phase varies from −50° down to −180° for the given CFRP specimen.

The typical convergence trends for the proposed hybrid method are shown in Fig. 4. It can be found from Fig. 4a, b that a sub-optimal solution can be obtained by SA at about No. of 35 iterations, and it is used as the initial-guess solution I. G. for the NM. The optimal solution of the fiber lay-up sequence estimation is quickly acquired by NM at about No. of 10 iterations, which indicates that the proposed hybrid method is readily employed to solve the objective function Eq. 16 to determine the fiber lay-up order of multilayer CFRP laminates. Table 1 presents the estimated results by five trails, and the estimation solution of each run is convergent to the global solution (the exact solution) by the hybrid method. Figure 5 shows the mean value and standard deviation of five running results. From Fig. 5, in this case, the maximum error of the fiber lay-up orientation angle is less than 5°, and the maximum standard deviation is

less than 4°. This indicates that the fiber lay-up orientation angle can be effectively identified by the proposed method using TWRI.

4 Conclusions

In this work, an inverse methodology that combines TWRI with numerical optimization technique is proposed to determine the fiber layer-up lamination sequences of anisotropic CFRP composite. The lock-in correlation between reference chirp signal and thermal-wave signal is developed. A hybrid algorithm that combines the SA with NM method is employed to solve the reconstructed cost function and find the global optimal solution of the layer-up sequences. Experimental results validate the feasibility of estimating the fiber layer-up lamination sequences of CFRP composite by the proposed method, and in this case, the maximum error of the fiber lay-up orientation angle is less than 5°.

Acknowledgments This work was supported in part by the Chinese National Natural Science Foundation under Grant No. 51173034, Self-planned Task of State Key Laboratory of Robotics and System (HIT) and the Program of Introducing Talents of Discipline of Universities (Grant No. B07108), and the authors are grateful to Spaceflight Materials and Technology Research Institute (SMTRI) for the specimen manufactured.

References

1. D.K. Hsu, F.J. Margetan, Adv. Compos. Lett. **2**, 51–55 (1993)
2. I.Y. Yang, K.H. Im, D.K. Hsu, V. Dayal, D. Barnard, J.H. Kim, C.S. Cha, Y.T. Cho, D.J. Kim, Compos. Sci. Technol. **69**, 2042–2047 (2009)
3. W. Karpen, D. Wu, G. Busse, Res. Nondestruct. Eval. **11**, 179–197 (1999)
4. R.J. Ball, D.P. Almond, NDT E Int. **31**, 165–173 (1998)
5. G. Kalogiannakis, D. Van Hemelrijck, S. Longuemart, J. Ravi, A. Okasha, C. Glorieux, J. Appl. Phys. **100**, 063521 (2006)
6. R. Mulaveesala, S.V. Ghali, Rev. Sci. Instruct. **82**, 054902 (2011)
7. J.Y. Liu, L.Q. Liu, Y. Wang, Compos. Part B Eng. **45**, 138–147 (2013)
8. C.I. Castanedo, M. Genest, S. Guibert, J.M. Piau, X.P. Maldague, A. Bendada, Proc SPIE **6541**, 654116 (2007)
9. I. Hatta, H. Yao, R. Kato, A. Macsono, Rev. Sci. Instrum. **56**, 1643–1647 (1996)
10. X.P. Maldague, *Theory and Practice of Infrared Technology for Nondestructive Testing* (Wiley, New York, 2001)
11. N.P. Avdelidis, D.P. Almond, Infrared Phys. Technol. **45**, 143–162 (2004)
12. N. Tabatabaei, A. Mandelis, B.T. Amaechi, Appl. Phys. Lett. **98**, 163706 (2011)
13. N. Tabatabaei, A. Mandelis, Phys. Rev. Lett. **107**, 165901 (2011)
14. H.S. Carslaw, J.C. Jaeger, *Conduction of Heat in Solid* (Oxford University Press, New york, 1959)
15. J.L. Gong, J.Y. Liu, L. Qin, Y. Wang, NDT E Int. **62**, 130–136 (2014)
16. J.Y. Liu, Q.J. Tang, Y. Wang, Compos. Sci. Technol. **72**, 1240–1250 (2012)
17. J.Y. Liu, J.L. Gong, L. Qin, B. Guo, Y. Wang, Int. J. Thermophys. **36**, 1226–1235 (2015)
18. J.Y. Liu, J.L. Gong, L. Qin, Y. Wang, Int. J. Thermophys. **36**, 1259–1265 (2015)
19. J.Y. Liu, F. Wang, Y. Liu, Y. Wang, Compos. Struct. **138**, 214–226 (2016)